29. Multiple Materials Melting (Germanium-Silicon Solid Solutions)

Part of Experiment MA-150*

V. S. Zemskov,[a] V. N. Kubasov,[a] I. N. Belokurova,[a] A. N. Titkov,[a] I. L. Shulpina,[a] V. I. Safarov,[a] and N. B. Guseva[a]

INTRODUCTION

An experiment on melting and directional crystallization of an antimony (Sb)-doped germanium (Ge) silicon (Si) solid solution was designed for the Apollo-Soyuz Test Project (ASTP) to study the possibility of using microgravity conditions for obtaining solid-solution monocrystals with uniformly distributed components. Solid-solution monocrystals obtained in a microgravity environment in the absence of buoyancy forces and thermal convection were expected to have a more homogeneous and even distribution of components compared to those obtained under normal gravity conditions.

It was anticipated that the absence of convectional mixing and the occurrence of mass transfer in the melt, caused by diffusion only, would create conditions for stationary crystal growth and would provide a compositional segregation consistent with these conditions (ref. 29-1). Also, in the absence of uncontrollable convective mixing, laminar distribution of components in a monocrystal is not likely to occur (ref. 29-2).

Antimony-doped Ge-Si solid solutions are favorable materials for studying the previously mentioned processes, because the distribution coefficient of Si in Ge ($K_{Si} > 1$) and that of Sb ($K_{Sb} < 1$) enable investigation of the behavior of components having different distribution coefficients. Also, because Sb-doped Ge-Si solid solution is a semiconducting material, the precision techniques that are widely used in studying semiconducting materials can be used for a detailed investigation of component distribution in crystal volume and for analyses of defects in crystal structure.

PREPARATION AND OPERATION OF THE EXPERIMENT

Cylindrical specimens (ingots) of Sb-doped Ge-Si solid solution were made of monocrystals obtained by means of crystal pulling from the melt, which was continually being fed with Si (ref. 29-3). All monocrystals had the following identical characteristics: <111> orientation growth, Si content from 0.7 to 1.0 at .%, Sb content from 1 to 2×10^{17} atoms/cm^3, dislocation density in the {111} face from 10^3 to 10^4 cm,$^{-2}$ laminar distribution of components with Si-content fluctuations in the layers ranging to 0.1 at.%, and heterogeneity associated with crystal face effect.

The monocrystals were ground so that the ingot diameter would not be smaller than the internal diameter of the quartz ampoule by more than 0.2 mm and so that the crystallographic <111> orientation would coincide with the ingot axis. The length of the ingot was 38 ± 0.1 mm.

*The Multiple Materials Melting Experiment is one of the five experiments that incorporated joint activities between the U.S. and U.S.S.R. crews. The joint U.S.-U.S.S.R. designation was "Experiment AS-3." The "metals" part of the experiment is reported in section 28.

[a]Institute for Metallurgy, U.S.S.R.

The tubes used to fabricate the ampoules were made of quartz that contained total impurities of not more than 1.2×10^{-3} wt%. Before inserting the ingots, the internal surface of each ampoule was coated with graphite by means of acetone pyrolysis.

A schematic diagram of an ampoule containing an ingot is shown in figure 29-1. To increase the mechanical strength of the ampoule, the walls of its rounded end (situated in the hot zone of the furnace) were made thicker than those of the remainder of the ampoule. The corresponding end of the ingot had a spherical shape matching the internal surface of the ampoule. At the other end of the ampoule, where sealing had to be performed, the specimen had a plane surface. Two spacers, which were of the same diameter as that of the specimen and which were made of high-purity graphite that had been additionally annealed in vacuum at a temperature of approximately 1773 K (1500° C), were located at the plane face; and another spacer consisting of four layers of quartz cloth was located between the two graphite spacers. The ampoules were sealed at 13.33 mN/m^2 (10^{-4} torr) to make the quartz tube press the graphite spacers tightly against the specimen.

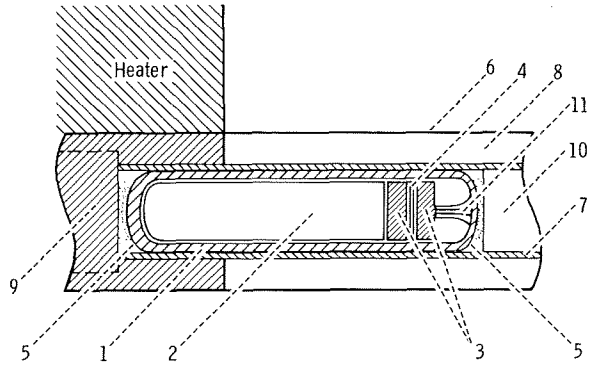

1. Quartz ampoule: outside diameter, 11.5 ± 0.1 mm; length, $52 \begin{smallmatrix} + 0.05 \\ - 1.0 \end{smallmatrix}$ mm
2. Ingot: diameter, 9.5 ± 0.1 mm; length, 38 ± 0.1 mm
3. Graphite spacers
4. Spacer consisting of four layers of quartz cloth
5. Copper foil
6. Stainless steel cartridge
7. Stainless steel tube
8. Heat insulation
9. Graphite insert for ampoule 1
10. Copper insert for ampoule 3
11. Quartz tube

FIGURE 29-1.—Schematic diagram of ampoule containing ingot of Ge-Si solid solution.

The ampoules with the ingots were transferred to the United States for insertion into cartridges of a specific design. Both ends of the ampoules were wrapped with copper foil to create the necessary conditions for heat transfer inside the cartridge.

The experiment on melting and crystallization of Ge-Si solid solution was conducted in the three-chamber multipurpose furnace (sec. 21). According to the experiment plan, the ampoule containing the solid solution was to be placed in the furnace gradient zone, in which the following thermal conditions were to be maintained.

1. A temperature of 1323 K (1050° C) at the hot end and a temperature of 973 K (700° C) at the cold end

2. A thermal gradient along the ampoule from 30 to 40 K/cm (30° to 40° C/cm) when the specimen was in a molten state, and from 10 to 40 K/cm (10° to 40° C/cm) during the cooldown phase

This temperature distribution in the gradient zone would be expected to restrict the melting of the ingot to no more than two-thirds of its length, so that the remainder of it served as a seed for crystallization of the melt.

For the purpose of developing the required thermal mode and perfecting the ampoule and cartridge designs, ground-based thermal simulation experiments using prototypes of the flight ampoules and furnace were conducted in the United States. These experiments helped to obtain the desired temperatures at the hot and cold ends of the furnace. However, during these experiments, the distribution of the temperature along the ampoules containing the solid solution was such that the thermal gradient did not exceed 20 K/cm (20° C/cm) at any point along the ingot. Under these thermal conditions, complete melting of the entire ingot could be expected.

During the experiment in the microgravity environment as well as during the ground-based thermal simulation tests, the temperature cycles were kept in conformity with the plan.

CRYSTAL-STUDY TECHNIQUES

Upon experiment completion, the first step (both in thermal simulation tests and during the mission) was an X-ray analysis of the cartridges to detect changes in their internal parts. Then, the cartridges were opened, and the surface, contour, and macrostructure of the crystals were visually inspected. Next, structural perfection of the crystals and the distribution of their components in longitudinal sections and cross sections were investigated.

For this purpose, the specimens were prepared and oriented by means of X-ray techniques so that their longitudinal and cross sections correspond to the planes that are appropriate for investigation; these are {110} and {100} planes. The preparation scheme for monocrystals grown in <111> orientation is presented in figure 29-2, where I and III designate the series of samples that was subjected to X-ray-topographical, spectral, electrophysical, and metallographic analyses and where II designates the series of samples for investigation of electrophysical properties.

To determine Si content in crystals, photoluminescence spectra were analyzed (refs. 29-4 to 29-6). Because the size of the investigated area was ≤ 0.11 mm^2, a high topographic resolution was obtained. The error in Si-content determination was ≤ 0.1 at.%. Specific resistance was measured by means of conventional four- and two-probe compensation techniques and by the spreading-resistance method (ref. 29-7).

The distribution of Sb along the crystals was determined by measurements of carrier concentration using the Hall-effect method. Samples for these measurements were cut out of the series II sections (fig. 29-2) in regions that were adjacent to the center of the crystal.

The crystal structure was investigated by means of the X-ray diffraction topography methods of Berg-Barrete-Newkirk and of Lang (ref. 29-8). For the Berg-Barrete-Newkirk method, a specific camera was used (ref. 29-9). This camera enables a crystal survey geometry capable of providing a linear resolution of 3 μm and an angular resolution of 5′ for copper Kα radiation. The depth of the crystal measurement layer was from 5 to 25 μm. For the Lang method, a standard

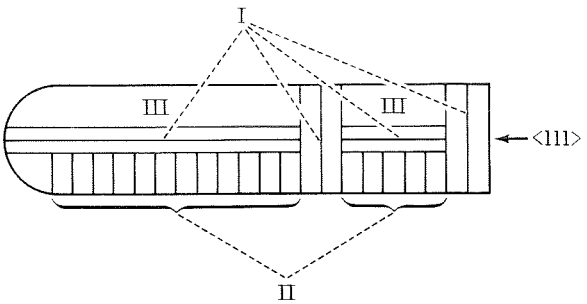

FIGURE 29-2.—Schematic of crystal-sample preparation.

camera with crystal scanning was used, and the linear resolution of molybdenum Kα radiation for this camera was 5 μm.

The detection of dislocations by means of chemical etching permitted an evaluation of microscopic and macroscopic heterogeneities of Ge-Si solid solutions in the investigated crystal face. Chemical etching was performed using ferricyanide etchant (ref. 29-10) on the {111} or the {110} face, which had been previously polished in CP-4A solution. A metallographic microscope with 90× or 120× enlargement was used to study the density of dislocations and their distribution in the etched crystal face.

RESULTS

Ingot Macrostructure

For the purpose of studying the microgravity (≤ 0.006g) effect on melting and crystallization of Ge-Si solid solution and comparing the results with those of other studies on identical crystals obtained under normal gravity conditions, four experiments on Earth and one in space were performed.

The postexperiment X-ray analysis of the flight cartridges revealed no damage to the internal parts of the cartridges; all the ampoules and crystals remained intact. A visual inspection of the crystals, after the cartridges had been opened, showed no macroirregularities, such as cracks, scratches, or cavities.

The results of a preliminary examination of the macrostructure of all crystals obtained under both normal gravity and microgravity conditions are summarized in table 29-I.

The photographs of space-grown crystals are shown in figure 29-3. From the contour of the crystals, a conclusion can be made that the ingot MA-150-16 melted completely and was measurably superheated. Both ends of the crystal had a typical spherical contour, which has never been observed in ground-based crystals. The entire surface of the ingot in cartridge MA-150-18 melted also, but the ingot was less superheated than MA-150-16. The ends of crystal MA-150-18 also had a spherical shape but with a smaller curvature radius compared to that of MA-150-16. An approximately 4-mm-long portion of ingot MA-150-17 appeared unmelted, supposedly an indication that this crystal preserved its seed. Subsequent etching of the crystals showed that MA-150-18 had a monocrystalline structure, whereas MA-150-16 and MA-150-17 were polycrystalline.

It should be noted that all space-grown crystals, both monocrystals and polycrystals, had a specific surface contour (fig. 29-4) never observed in ground-based crystals. Such a contour would indicate that wetting of the graphite-coated ampoule walls by the melt does not occur during crystallization under microgravity conditions.

Two groups of crystals, each containing two ingots, were selected for subsequent measurements. The basic data on these crystals are given in table 29-II.

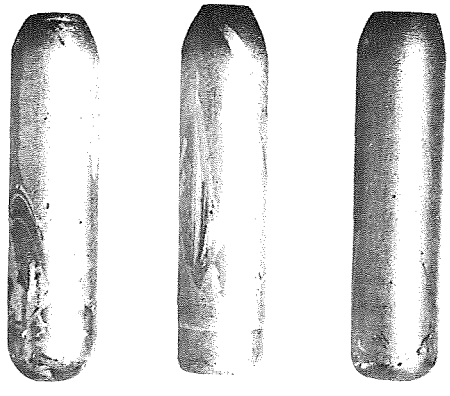

FIGURE 29-3.—Photographs of space-grown crystals.

TABLE 29-I.—Results of External Examination of Ge-Si Solid-Solution Crystals Obtained During Ground-Based Experiments and Under Microgravity Conditions

Cartridge no.	*Melted portion of ingot, percent*	*Structure*
	Ground-based experiment 1	
MA-150-01	100	Polycrystalline
MA-150-02	100	Polycrystalline
MA-150-03	100	Polycrystalline
	Ground-based experiment 2	
MA-150-04	--	--
MA-150-05	100	Polycrystalline
MA-150-06	100	Monocrystalline
	Ground-based experiment 3	
MA-150-07	100	Monocrystalline
MA-150-08	100	Monocrystalline
MA-150-09	100	Polycrystalline
	Ground-based experiment 4	
MA-150-10	(a)	(a)
MA-150-11	60	Monocrystalline
MA-150-12	80	Monocrystalline
	Space-grown	
MA-150-16	100	Polycrystalline
MA-150-17	90	Polycrystalline
MA-150-18	100	Monocrystalline

[a]Was not melted; opened after dynamic tests.

Monocrystals Obtained Without Seeding

Silicon distribution.—Silicon distribution in space-grown monocrystal MA-150-18 is shown in figure 29-5. Figure 29-5(a) shows Si distribution along one edge of the crystal; figure 29-5(b), along the other. As indicated in figure 29-5, a decreasing Si content with increasing distance from the point of original crystallization is the basic characteristic of impurities with $K > 1$. A considerable scattering of Si concentration was noticed in the initial region of the crystal. It is also evident from figure 29-5 that the Si distribution across the crystal diameter was nonuniform. This nonuniformity

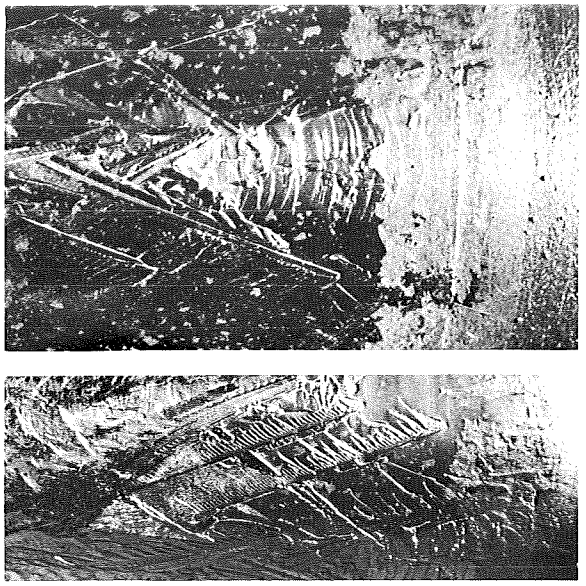

FIGURE 29-4.—Surface of space-grown crystal MA-150-17; areas near the seed.

across the crystal was decreasing toward the end of the crystal. Silicon distribution in the longitudinal section through the center of the crystal is not shown, but it was similar to that shown in figure 29-5(a). The Si distribution throughout the diameter of ground-based crystal MA-150-07, in regions located close to the onset and termination of crystallization, proved to be virtually uniform and, by its form, in agreement with the laws of normal directional crystallization (fig. 29-6).

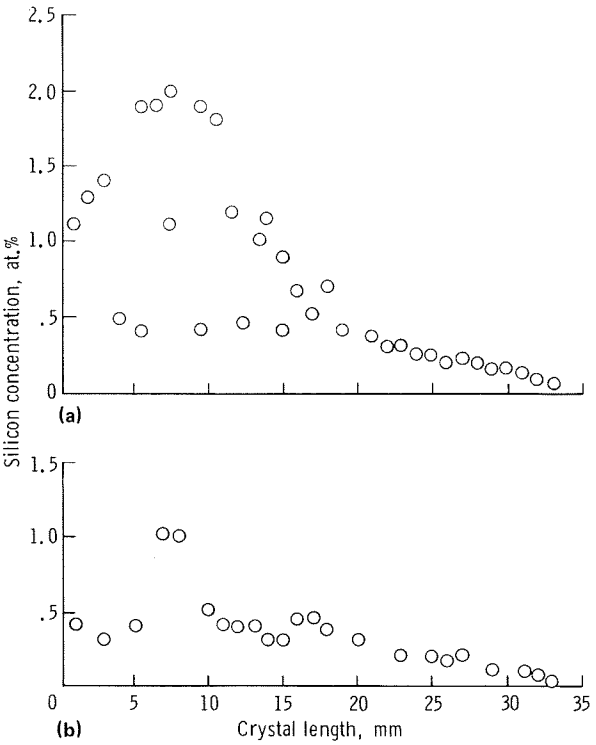

FIGURE 29-5.—Silicon distribution in space-grown monocrystal MA-150-18. (a) Left side of crystal. (b) Right side of crystal.

Antimony distribution.—The changes in specific resistance along space-grown crystal MA-150-18 and ground-based crystal MA-150-07, measured on series II samples (fig. 29-2), are shown in figure 29-7. The specific resistance of the space-grown

TABLE 29-II.—Basic Data on Crystals Selected for Measurements

Crystal no.	*Growth conditions*	*Presence of seed*	*Orientation*	*Remarks*
		Group I		
MA-150-18	Space	No	<110>	
MA-150-07	Ground	No	<100>	
		Group II		
MA-150-17	Space	Yes	<111>	4-mm-long seed
MA-150-12	Ground	Yes	<111>	7-mm-long seed

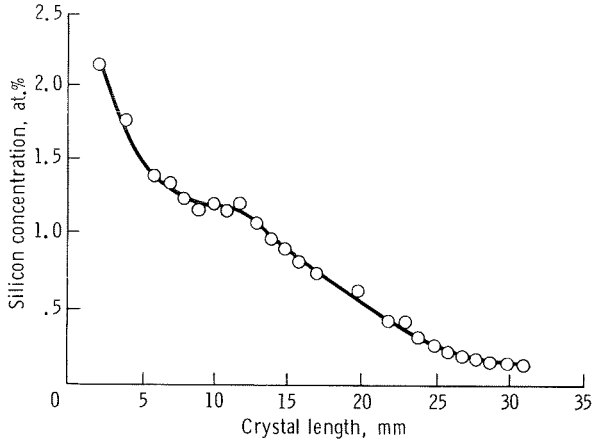

FIGURE 29-6.—Silicon distribution in ground-based monocrystal MA-150-07.

crystal remained virtually constant along approximately 20 mm and decreased abruptly only at the end of the crystal, whereas the specific resistance of the ground-based crystal decreased monotonically from the beginning to the end of the crystal. Consequently, the nature of the changes indicates that Sb distribution was uniform throughout a large portion of crystal MA-150-18.

Antimony-content determination by measurements of carrier concentration performed using the Hall-effect method showed that, in crystal

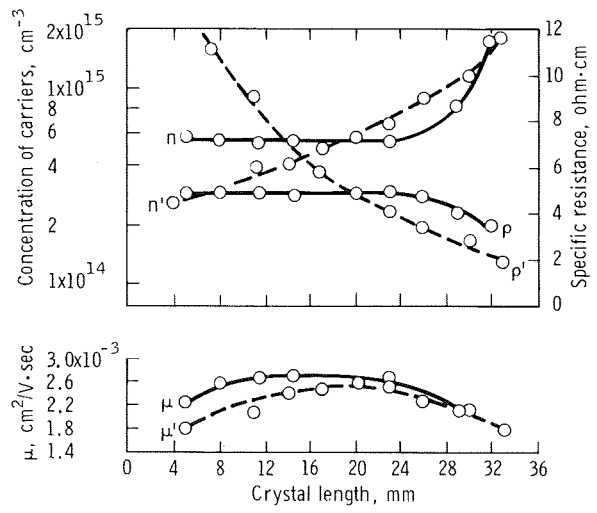

FIGURE 29-7.—Change in specific resistance, in concentration, and in mobility of charge carriers for crystals MA-150-18 (ρ, n, and μ, respectively) and MA-150-07 (ρ', n', and μ', respectively).

MA-150-18, Sb was distributed uniformly (fig. 29-7), whereas, in the ground-based crystal MA-150-07, the concentration of Sb increased along the entire length of the crystal from the beginning to the end. It is interesting to note that such uniformity of Sb distribution, which occurred during Ge-Si solid-solution crystallization under microgravity conditions, has never been obtained under Earth conditions except when special techniques capable of providing uniform distribution of impurities in a crystal were used.

An analysis of charge-carrier-distribution curves showed that Sb concentration in the area with uniform Sb distribution in the space-grown crystal was approximately 6×10^{14} atoms/cm^3, whereas it could have been equal to Sb concentration in the melt (i.e., $\approx 2 \times 10^{17}$ atoms/cm^3) if ideal stationary conditions of growth and segregation, depending only on the diffusion in the melt near the crystallization front, were obtained in the microgravity environment. On the other hand, the value $\approx 6 \times 10^{14}$ atoms/cm^3 is in good agreement with the value of the Sb-distribution coefficient if one accepts that this coefficient is equal to the coefficient of Sb distribution in Ge (3×10^{-3}) for a solid solution low in silicon and that the crystal grows from a melt with an Sb concentration of $\approx 2 \times 10^{17}$ atoms/cm^3, which is approximately the Sb concentration in the original ingot.

Changes in the Hall mobility of charge carriers along both space-grown crystals and ground-based crystals were similar (fig. 29-7). However, the distribution of Sb throughout the space-grown crystal was nonuniform, Sb concentration changing from one edge of the cross section to the other by two or three times. The nonuniformity was obvious from measurements of specific resistance of crystal MA-150-18 along its three parallel lines (going along the edges and the center of the crystal) and from the nature of spreading-resistance changes in the cross sections.

Crystal structure.—Monocrystals MA-150-07 and MA-150-18 had a dendritic structure as the crystal first solidified (figs. 29-8(a) and 29-8(b)); as crystallization continued, the dendritic structure changed to a block structure (figs. 29-9(a) and 29-9(b)). This transition is clearly indicated in photographs of the longitudinal section of the region of initial crystallization (figs. 29-10(a) and

(a)

(b)

FIGURE 29-8.—X-ray topographs of cross sections of the initial regions of crystals MA-150-07 and MA-150-18 (8×). (a) MA-150-07 (ground based). (b) MA-150-18 (space grown).

(a)

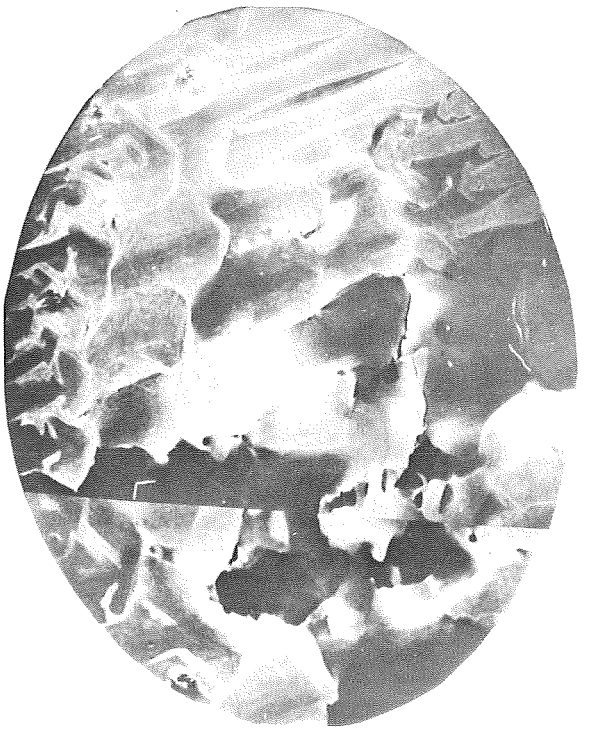

(b)

FIGURE 29-9.—X-ray topographs of cross sections of the central regions of crystals MA-150-07 and MA-150-18 (8×). (a) MA-150-07 (ground based). (b) MA-150-18 (space grown).

29-10 (b)). Both space-grown and ground-based crystals had zones of local deformation centers, located mainly in the region of initial crystallization and concentrated near the lateral surface of the crystals (figs. 29-10(a) and 29-10(b)); whereas the central portion of the crystals was almost completely free of such defects. However, an extensive region of microstresses, caused probably by local deformation centers, was observed in the central part. Crystal MA-150-18 had a different number of local deformation centers near different lateral surfaces. The reason for these defects could be the trapping of separate drops of the melt caused by irregular crystal growth, an indication of the presence of microheterogeneities in the composition of the crystal.

Blocks in different cross sections along the length of crystals differed in size and orientation. This difference can be attributed to microheterogeneities in the composition of the solid solution resulting from radial thermal gradients in the multipurpose furnace.

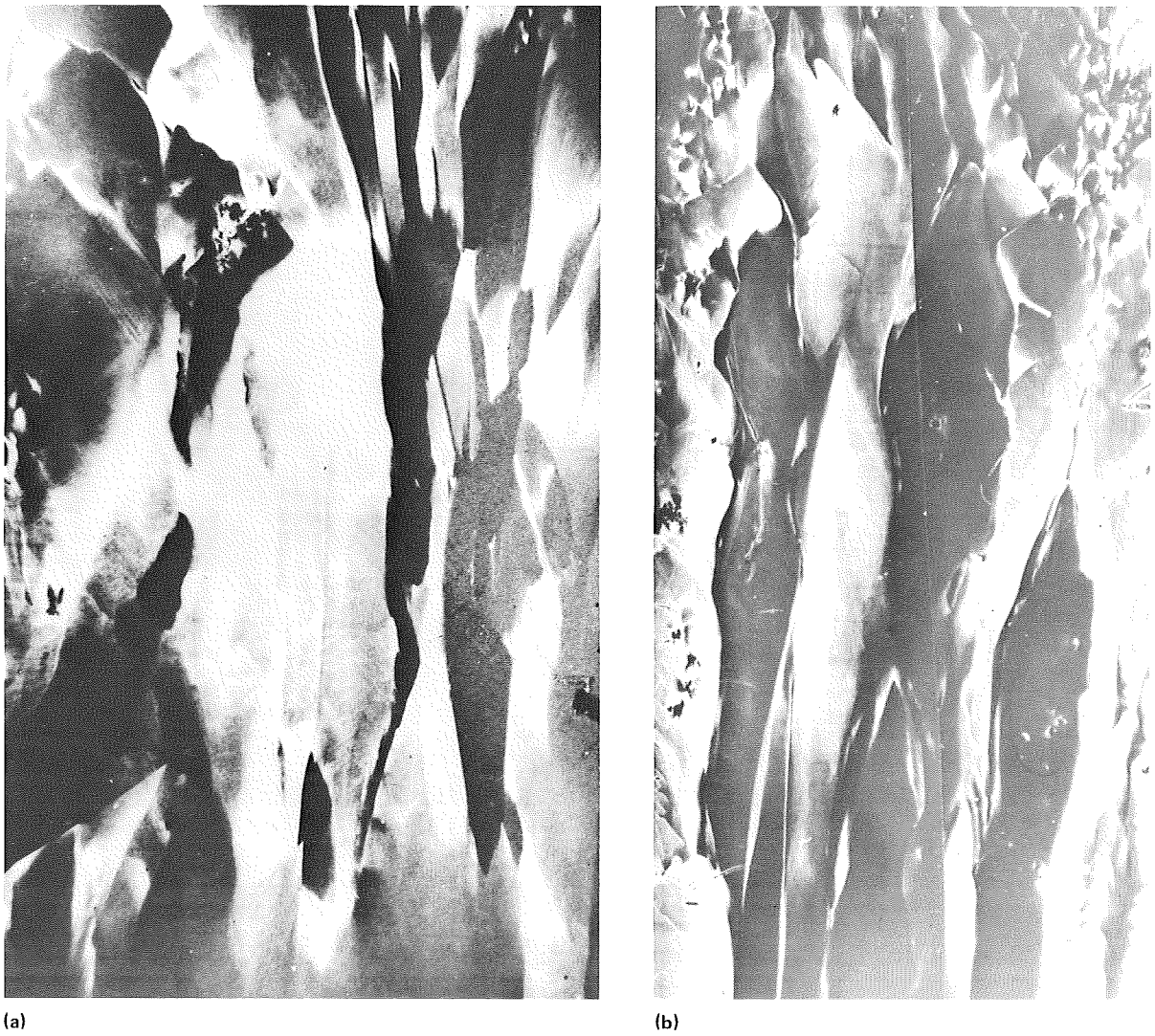

FIGURE 29-10.—X-ray topographs of the longitudinal sections of crystals MA-150-07 and MA-150-18 (10×). (a) MA-150-07 (ground based). (b) MA-150-18 (space grown).

(a)

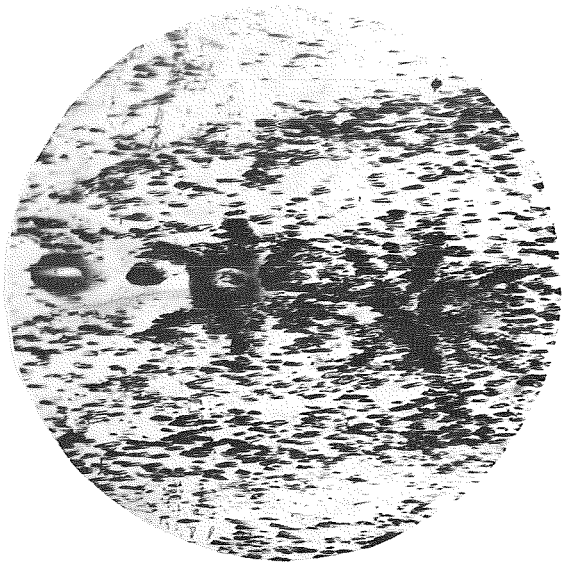

(b)

FIGURE 29-11.—Distribution of dislocations and centers of local deformation in {110} plane of the longitudinal section of crystal MA-150-18. (a) Distribution of dislocations. (b) Centers of local deformation.

Photomicrographs in figures 29-11 and 29-12 show the distribution of dislocations in {110} planes of the longitudinal section and cross section of monocrystal MA-150-18. A region with a high density of dislocations (i.e., a region that had the most heterogeneous Si distribution) was observed at the beginning of crystallization, where Si content was the highest. Distribution of dislocations throughout the longitudinal section of this portion of the crystal (fig. 29-11(a)) was in keeping with its structure, as shown by X-ray diffraction topography (fig. 29-10(b)). Local defects are clearly indicated in this region (fig. 29-11(b)). With an Si-content decrease, the density of dislocations diminished, and their distribution throughout the longitudinal section became more uniform.

A cellular structure, which indicates the presence of constitutional supercooling at the front of crystallization, is clearly indicated in the cross section of the central part of the crystal (fig. 29-12). (The X-ray topograph is given in fig. 29-9(b)).

Crystals Obtained With Seeding

Silicon distribution.—The change in Si content throughout ground-based crystal MA-150-12, which had an approximately 7-mm-long seed, is shown in figure 29-13. The curve is composed of several segments that characterize the recrystallization process. The initial segment of the Si-distribution curve corresponds to the approximately 7-mm-long unmelted part of the ingot, which served as a seed for crystallization. Silicon concentration in this region was constant and equaled 0.7 at.%. At the interface of melting and subsequent crystallization, Si concentration

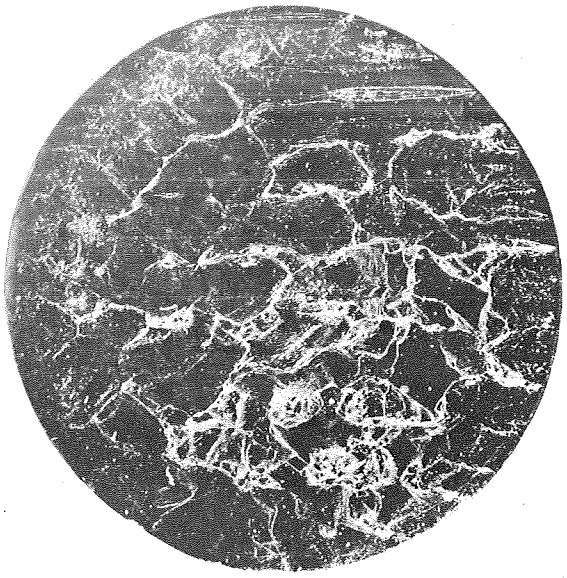

FIGURE 29-12.—Distribution of dislocations in {110} plane of the cross section of crystal MA-150-18.

abruptly increased to a value of 1.6 at.%. In the remaining part of the crystal, the concentration of Si decreased gradually as the crystallization of the melt was in progress. In the ground-based experiment, the effective coefficient of Si distribution in Ge during crystallization was evaluated from the curve in figure 29-13. The value of 2.3 agrees with published data on values of K for nonequilibrium conditions of crystallization. The Si distribution throughout the cross sections of the crystal was practically uniform, varying by no more than 20 percent.

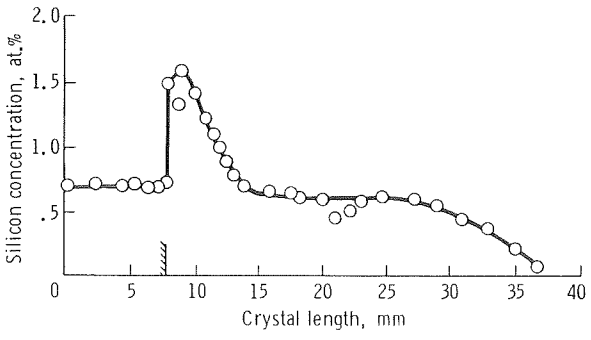

FIGURE 29-13.—Silicon distribution in ground-based crystal MA-150-12.

Silicon distribution in the region of the seed of space-grown crystal MA-150-17 is unusual (fig. 29-14). An increase in Si concentration is observed in two regions, in that of the seed and in that located at some distance from the crystallization boundary. In the section between the two regions, approximately 2 mm long, Si concentration could not be estimated. The anomalous change of composition in the region of the seed can be attributed to regeneration of the seed; namely, to melting of localized areas.

Silicon distribution throughout the cross section of the recrystallized region, which had a polycrystalline structure, was identical to that of the space-grown monocrystal MA-150-18. A change in Si concentration from one edge toward the other was observed in both crystals.

Antimony distribution.—Changes in specific resistance and charge-carrier concentration throughout the length of crystals grown with seeding, both under microgravity (MA-150-17) and Earth (MA-150-12) conditions, are shown in figure 29-15. The curves for specific resistance and carrier concentration in the crystals were of the same type as those for monocrystals grown without seeding, except for the region of the seed. The seed region of crystal MA-150-12 had the same specific resistance and carrier concentration as the original ingot. The space-grown crystal MA-150-17 had the same specific resistance value as the original ingot only in the end face that was adjacent to the graphite spacer and was located in

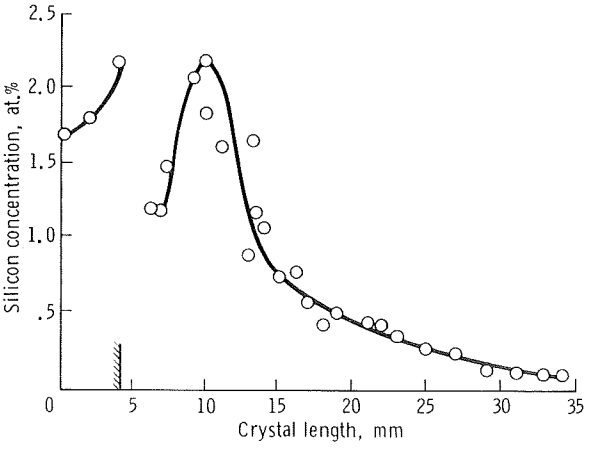

FIGURE 29-14.—Silicon distribution in space-grown crystal MA-150-17.

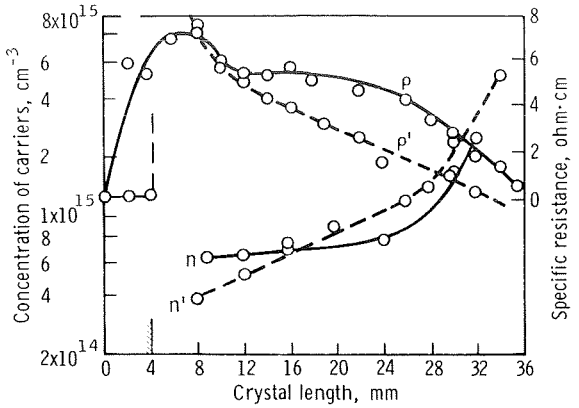

FIGURE 29-15.—Changes in specific resistance and charge-carrier concentration for crystals MA-150-17 (ρ and n, respectively) and MA-150-12 (ρ' and n', respectively).

the cold end of the furnace. Strictly speaking, it was only this zone that served as a seed. After that zone, the specific resistance increased abruptly in a 4-mm-long region with an outward contour of a seed. The increase in specific resistance and the nature of Si distribution in this region indicate that, although the seed preserved its original contour, it probably underwent partial melting and recrystallization during the experiment.

Crystal structure.—The most interesting part of the investigation of the structure of space-grown crystal MA-150-17 was the study of the structure of its seed in comparison with the structure of the seed and the region of original recrystallization in ground-based ingot MA-150-12.

Figure 29-16(a) shows the outward appearance of the portion of crystal MA-150-12 that includes the seed, the boundary of melting, and the recrystallized part of the crystal, the diameter of which was somewhat larger than that of the seed. The distribution of dislocations in the {110} plane is shown in figure 29-16(b), and the X-ray topograph of the seeding boundary of this crystal is shown in figure 29-17.

The crystallization interface had a concave (in the direction of the seed) shape and a steplike structure. The region near the crystallization interface had a high density of dislocations and numerous centers of local deformation. The X-ray topography revealed a laminar structure of the seed that was not observed in Ge-Si solid-solution

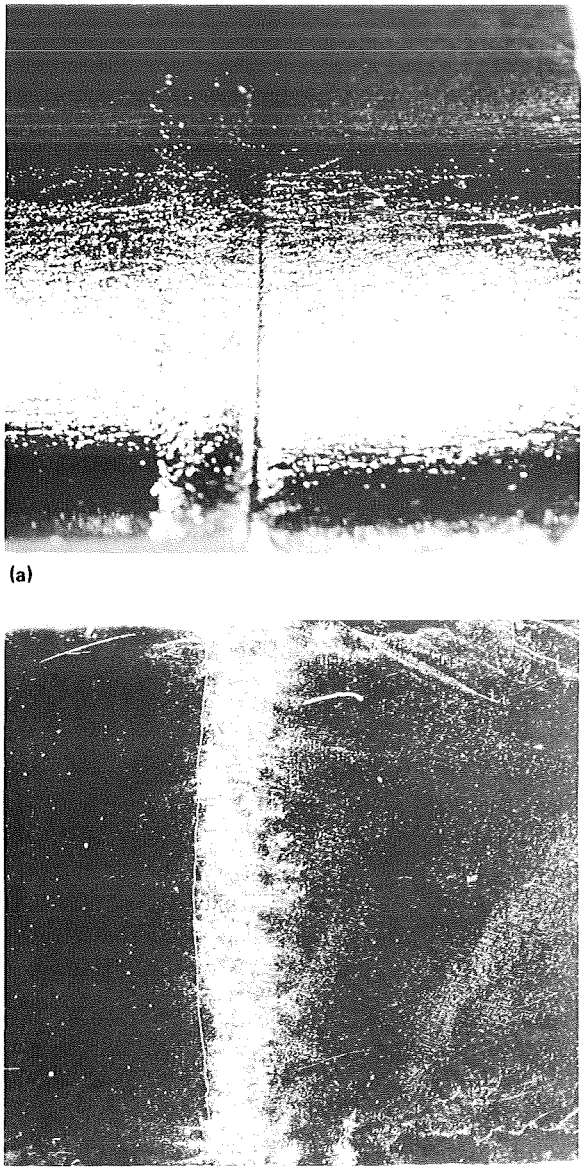

FIGURE 29-16.—Region of the seeding boundary of crystal MA-150-12. (a) Outward appearance. (b) Distribution of dislocations.

monocrystals obtained under microgravity conditions.

The outward appearance of the end of crystal MA-150-17 is shown in figure 29-18(a). The figure shows a sharp boundary line between the seed and the recrystallized portion, which, similar to that of crystal MA-150-12, has a slightly enlarged

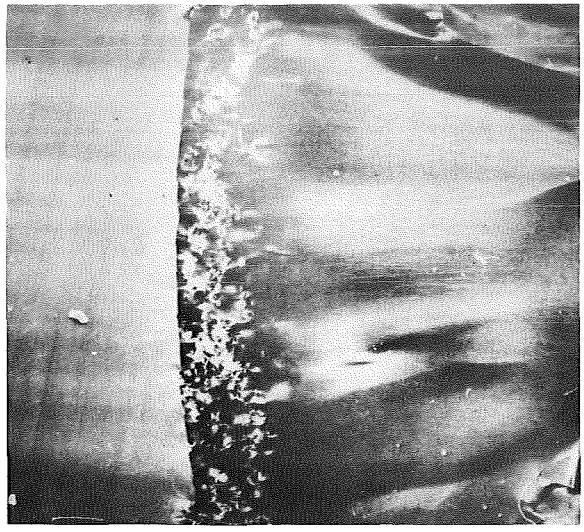

FIGURE 29-17.—X-ray topograph of the seeding boundary region of crystal MA-150-12 (9×).

diameter. However, the macrostructure and the X-ray topograph of this region (figs. 29-18(b) and 29-19) are fundamentally different from those of the ground-based crystal (figs. 29-16(b) and 29-17). The region of the seed in crystal MA-150-17 is of a heterogeneous structure characterized by centers of local deformation located close to each other. Outside this region, local deformation centers are not observed everywhere but in single groups. Furthermore, formation of a block structure with strong microstresses and macrostresses occurred, and the monocrystal changed to a polycrystal.

A detailed investigation of the seed indicated that portions of its surface, which were adjacent to the graphite spacer, began melting in hexagonal patterns (fig. 29-20(a)). The center of the seed surface was distorted. An X-ray topograph of the surface of a sample taken from the opposite end of the seed (fig. 29-20(b)) indicated that, following the hexagon corners, other portions of the crystal along the hexagon sides started melting; but the melting occurred locally, in isolated areas only. The spreading of the melting throughout a section of the crystal is shown in figure 29-20(c), which is a photograph of that portion of the seed adjacent to the region shown in figure 29-19. It should be noted that the radial spreading of the melting regions was unsymmetrical. Considering that

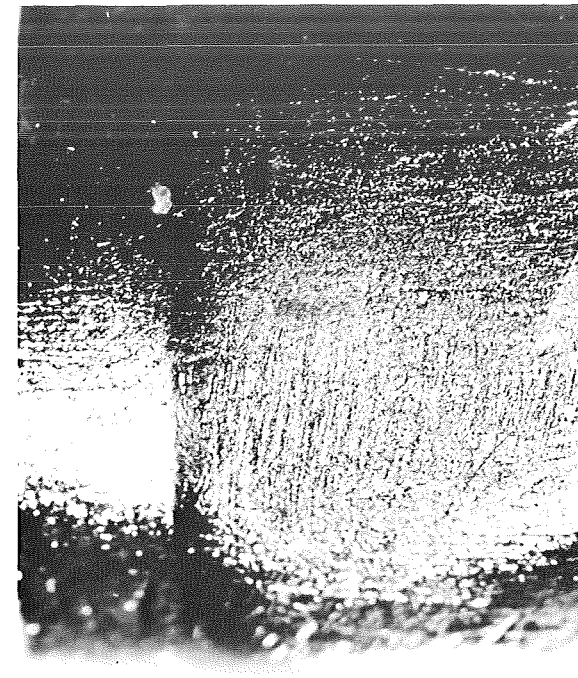

(a)

(b)

FIGURE 29-18.—Region of the seeding boundary of crystal MA-150-17. (a) Outward appearance. (b) Distribution of dislocations.

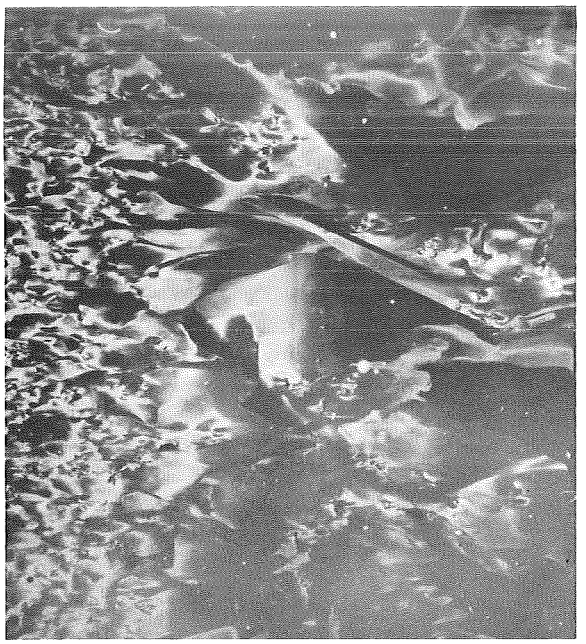

FIGURE 29-19.—X-ray topograph of the seeding boundary region of crystal MA-150-17 (9×).

(a)

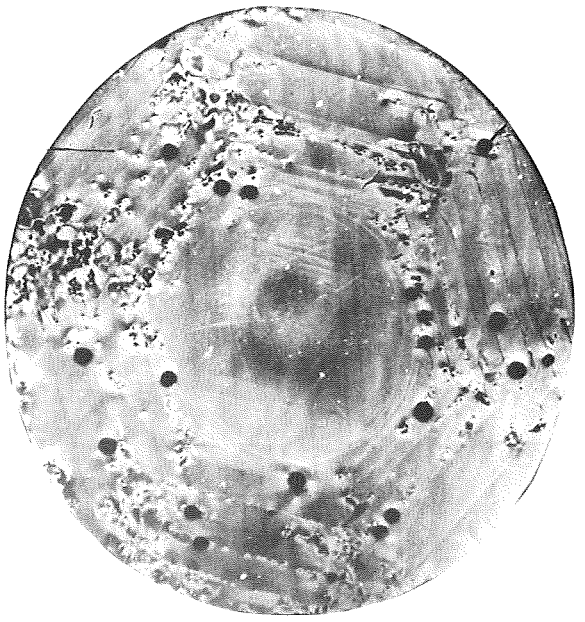

(b)

(c)

FIGURE 29-20.—X-ray topographs of space-grown crystal MA-150-17 (8×). (a) Seed surface adjacent to graphite spacer. (b) Opposite side of specimen shown in figure 29-20(a); thickness of specimen, ≈1 mm. (c) Seed surface adjacent to the region of crystal MA-150-17 shown in figure 29-19.

microheterogeneities of Si distribution in the layers of the original ingot were ≈0.1 at.%, it was possible to determine the thermal gradient of the seed region in the longitudinal direction and across the crystal by the size of the regenerated seed. The gradient was approximately 1 K/cm.

Thus, crystal MA-150-17, obtained under microgravity conditions, had no recrystallization boundary. Recrystallization started gradually (2 to 3 mm behind the line visible on the outward surface) and developed consecutively both along the crystal growth and in the radial direction.

CONCLUSIONS

The investigation of Ge-Si solid-solution crystals obtained under microgravity conditions in the ASTP multipurpose furnace experiment gave the following results.

1. Under microgravity conditions, monocrystals of Sb-doped Ge-Si solid solution were obtained with and without seeding by means of directional crystallization in ampoules.

2. The analysis of Si and Sb distribution in crystals and of their structures has resulted in a series of conclusions concerning melting and crystallization under microgravity conditions.

3. During melting and crystallization under microgravity conditions, convective mixing is either absent or sufficiently negligible to have no effect on the process. The following facts support this conclusion.

a. Laminar distribution of crystal components was absent.

b. Cellular structure, which indicates the presence of constitutional supercooling at the crystallization front, was observed.

c. Regeneration of the seed occurred in the microgravity environment only (in the absence of mixing); complete melting without regeneration of the seed would have occurred under Earth conditions.

4. Crystallization in the microgravity environment did not occur under ideal stationary growth and segregation conditions, which could have been expected considering that directional crystallization occurs in the absence of convective mixing.

5. Crystallization under microgravity conditions revealed the heterogeneous nature of Si and Sb distribution in the cross sections of crystals. The presence of the radial thermal gradient in the multipurpose furnace could be one of the reasons for such Si and Sb distribution.

6. The structure of space-grown crystals correlates with the nature of heterogeneities of Si and Sb distribution in crystals.

7. The type of surface morphology and the contour observed in space-grown crystals have never been observed in ground-based crystals and indicate the absence of wetting of the graphite-coated walls of the ampoule by the melt during melting and crystallization.

8. All original ingots melted completely, an indication that the temperature distribution along the ampoule containing Ge-Si solid solution did not satisfy the optimal conditions planned for the experiment. In the area where the cold end of the ampoule was located and where a part of the ingot had to stay unmelted to serve as a seed, the temperature was 1211 K (938° C) and higher.

9. The regeneration of the seed proves that the thermal gradient in the region of the seed was not higher than 1 K/cm, causing local melting of the seed, a change in its structure, and the formation of a polycrystalline structure during subsequent crystallization. Such thermal conditions were unfavorable for the growth of monocrystals.

REFERENCES

29-1. Tiller, W. A.; Jackson, K. A.; Rutter, J. W.; and Chalmers, B.: The Redistribution of Solid Atoms During the Solidification of Metals. Acta Met., vol. 1, no. 4, 1953, pp. 428-437.

29-2. Lodiz, R.; and Parker, R.: Rost monokristallov. (Monocrystal Growth.) MIR Press (Moscow), 1974, pp. 522-524.

29-3. Belokurova, I. N.; Kekua, M. G.; Petrov, D. A.; and Suchkova, A. D.: Growth of Single Crystals of Germanium-Silicon Alloys. Izvest. Akad. Nauk S.S.S.R., Otdel, Tekh. Nauk, Met. i Toplivo, vol. 1, 1959, pp. 9-12.

29-4. Gross, E. F.; Sokolov, N. S.; and Titkov, A. N.: Zero-Phonon Radiative Annihilation of Indirect Excitons in Germanium Crystals with Isoelectronic Substitutional Impurities. Soviet Phys. - Solid State, vol. 14, no. 7, 1973, pp. 1732-1734.

29-5. Pokrovskii, Ya. E.; Svistunova, K. I.; and Alkeev, N. V.: Effect of Band Structure on the Recombination Mechanism of Condensed Charge Carriers in Germanium, Silicon, and Their Alloys. Soviet Phys. - Solid State, vol. 14, no. 11, 1973, pp. 2805-2807.

29-6. Safarov, V. I.; and Titkov, A. N.: Indirect Phonon-Free Optical Transitions in Germanium-Silicon Solid Solutions. Soviet Phys. - Solid State, vol. 14, no. 2, 1972, pp. 380-383.

29-7. Gupta, D. C.; and Chan, J. Y.: A Semiautomatic Spreading Resistance Probe. Rev. Sci. Instrum., vol. 41, no. 2, Feb. 1970, pp. 176-179.

29-8. Pryamyye metody issledovaniya defektov v kristallakh. (Direct Methods of Crystal-Defect Studies.) MIR Press (Moscow), 1965, pp. 7-23 and 205-222.

29-9. Gross, Ya. G.; Pokornyi, E. G.; et al.: X-Ray Camera for Investigating Defects in Crystals. Instrum. & Exp. Tech., vol. 15, no. 4, 1972, pp. 1246-1248.

29-10. Travleniye poluprovodnikov. (Etching of Semiconductors.) MIR Press (Moscow), 1965, pp. 184-187.